# Tillandsia-inspired Composite Materials for Atmospheric Water Harvesting

*An Feng,[a] Shudi Mao,[a] Casey Onggowarsito,[a] Gayathri Naidu,[a] Wen Li [b] and Qiang Fu[a,*]*

[a] *Centre of Technology in Water and Wastewater, School of Civil and Environmental Engineering, University of Technology Sydney, NSW 2007, Australia.*

[b] *International Joint Laboratory of Biomimetic & Smart Polymers, School of Materials Science and Engineering, Shanghai University, Nanchen Street 333, Shanghai 200444, China*

** Corresponding author at: Centre of Technology in Water and Wastewater, University of Technology Sydney, NSW 2007, Australia. Email address: qiang.fu@uts.edu.au (Q. Fu)*

*KEYWORDS: Nonwoven fiber, PAEtMA, Free radical polymerization, Water shortage, Sunlight irradiation*

ABSTRACT

Atmospheric water harvesting (AWH) is a potentially promising small-scale approach to alleviate water crisis in arid or semi-arid regions. Inspired by the asymmetric structure of tillandsia leaves, a plant species native to semi-arid regions, we report the development of a bio-inspired composite (BiC) to draw moisture for AWH applications. With the advent of the post-COVID era, the nonwoven materials in used masks are discarded, landfilled or incinerated along with the masks as medical waste, and the negative impact on the environment is inevitable. The nonwoven sheet has porosity, softness and certain mechanical strength. We innovatively developed BiCs, immobilizing hygroscopic salt with a nonwoven mask for fast vapor liquefaction, and using a polymer network to store water. The resulting BiC material manages to achieve a high-water adsorption capacity of 1.24 g $g^{-1}$ under a low-moderate humidity environment and a high-water release ratio of ca. 90% without the use of photothermal materials, while maintaining high structural integrity in cyclic testing.

## INTRODUCTION

The earth has inexhaustible water resources, yet only 2.5% of the earth's total water resources are freshwater. Among them, 0.3% of surface freshwater is distributed in the atmosphere in the form of water vapor, accounting for $2\times10^{10}$ $m^3$, which is a considerable freshwater resource that has attracted increasing attention in recent years[1-3]. Capturing water from the air is known as atmospheric water harvesting (AWH) process[4, 5]. Water harvesting strategies can be divided into active condensation and passive condensation. Active condensation is arguably more efficient in water collection, however this strategy typically consumes secondary energy and/or chemical refrigerants. Passive condensation is considered to be an ideal energy-saving altenative.[6, 7]

Nature is the best designer. Tillandsia, an air plant that grows in arid regions, has evolved a special physiological structure to adapt to the arid climate.[8, 9] In detail, the "leaves" of the air plant are fleshy stems tightly surrounded on the surface by stomata and spike-like structures growing around the stomata (see Supporting Information Figure S1). At night, the tip of the spike array can liquefy the water vapor in the air, and the liquefied water droplets can gather around the stomata driven by the Laplace gradient and be absorbed by the fleshy stem, making it survive in harsh environments.[10] Unfortunately, most of the artificial AWH materials based on hydrogels or metal-organic frameworks (MOFs) are arguably to have insufficient vapour liquefaction ability.[11, 12] Although researchers have incorporated hygroscopic salts into these materials to enhance their water adsorption capacity under ambient conditions, the strong affinity of hygroscopic salts for water molecules in turn leads to reduced water release/production efficiency.[13, 14] For example, Li et al. reported a PAM-based hydrogel

containing calcium chloride and carbon nanotubes, with a maximum water adsorption capacity of 2.05 g $g^{-1}$ and a low desorption efficiency of 55%.[15] The trade-off between water uptake (under low-mediate humidity) and water release efficiency under ambient conditions limit the practical applications of artificial AWH materials. We thus saw this as an opportunity to engineer a Tillandsia-inspired AWH material to improve the water production in low to moderate humidity conditions.

The surface of the Tillandsia leaves liquefy water vapor at night, and the liquefied water is quickly transferred to the underlying storage layer for Tillandsia's survival needs. Inspired by the asymmetric structure of Tillandsia ‘leaves’, we developed a novel bioinspired composite (BiC) consisting of a hygroscopic salt-containing nonwoven layer and a hydrogel network for efficient AWH application. The resulting BiC material can utilize diurnal temperature difference to condense water vapour at night and then produce liquid water through evaporation-condensation during the hot day. Under a low-moderate humidity environment, the BiC composite exhibits an outstanding water adsorption capacity and a high water release ratio without the use of conventional photothermal materials (PTMs). The study thus reports a new avenue to develop biomimetic materials for practical AWH applications.

## RESULTS AND DISCUSSION

With the advent of the post-COVID era, the nonwoven materials in used masks are discarded, landfilled or incinerated along with the masks as medical waste, and the negative impact on the environment is inevitable. The nonwoven sheet has porosity, softness and certain mechanical

strength, making it an ideal container for hygroscopic salts. Therefore, we innovatively employed nonwoven mask to immobilize hygroscopic salts.

In this work, we prepared a series of BiC materials for AWH application and recycling of disposable masks. As shown in Scheme 1, polyethylene terephthalate (PET) nonwoven sheets with hydrophilic surface obtained from commercially available masks, were first immersed in hygroscopic salt solution (e.g. $CaCl_2$) and dried in oven. Then, a poly[2-(acryloyloxy)ethyl]trimethylammonium chloride (PAEtMA)-based hydrogel network contained 20 wt% polymer content were synthesized via free radical polymerization[16] and the nonwoven sheets were gently placed on the surface of the hydrogel during the gelation process (Step 2) to afford the BiC materials.

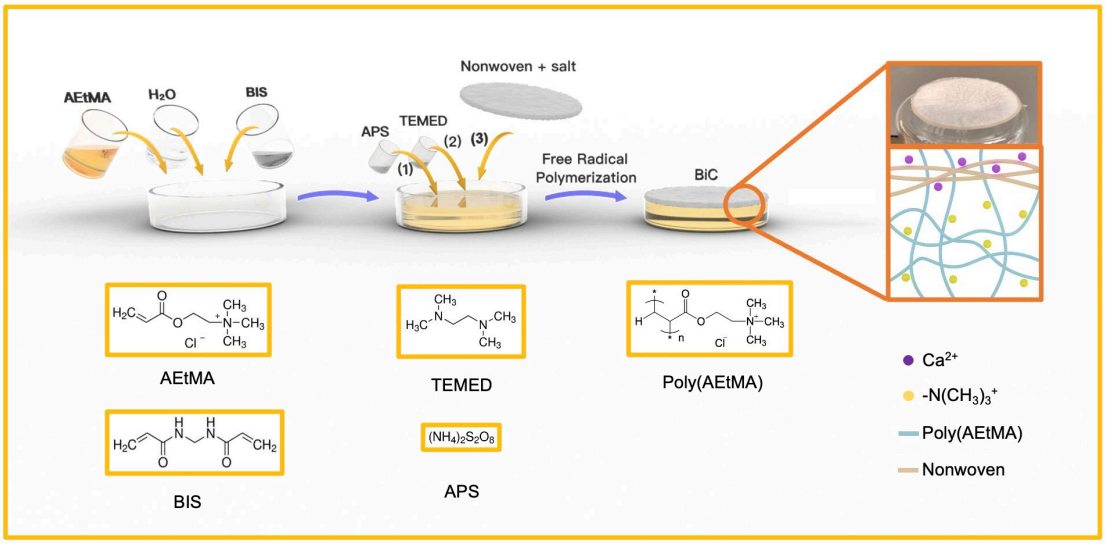


**Scheme 1.** Schematic illustration of the synthesis of composite AWH material.

We employed a nonwoven sheet to immobilize hygroscopic salts and constructed a polymer

hydrogel layer underneath. The porosity and huge swelling ratio of the PAEtMA network allow the water liquefied by $CaCl_2$ to pass through the polymer network from the nonwoven sheet via capillary force, thereby realizing the separation of the functions of vapor liquefaction and water storage in BiC materials to achieve high water adsorption and efficient water release. It is worth noting that although the treated non-woven sheet exhibits a strong rapid moisture adsorption capacity, as the vapor pressure of the calcium chloride solution increases with the increase in water adsorption, the evaporation and dissolution of water molecules will quickly reach a dynamic balance. This leads to the inability of the treated nonwoven sheet to store liquid water in large quantities. Therefore, the existence of the PAEtMA polymer network becomes a necessary condition for BiC to achieve high water adsorption capacity. This will be discussed further later.

We firstly characterized the surface morphology of the prepared BiC materials. We can clearly identify the rough nonwoven side and the relatively smooth hydrogel side using naked eye (Figure 1A-i-iii). After freeze drying, the nonwoven sheet was still closely connected with the PAEtMA hydrogel layer, and no obvious cracks were found at the interface (Figure 1A-iv). The microstructures of the surface of the nonwoven sheet, and the surface and cross-section of the PAEtMA network were characterized by SEM measurements (Figure 1B). We observed that the fibres of nonwoven sheet have a diameter of ca. 10 μm (Figure 1B-i). The unique microstructure of the nonwoven sheet provides large surface area for $CaCl_2$ immobilization and moisture liquefaction. In addition, the rough nonwoven surface offers large contact area to PAEtMA polymer network, improving interfacial connection. The polymer network has porous

morphology, which is confirmed by both surface and cross-section images in Figure 1B-ii and iii) respectively.

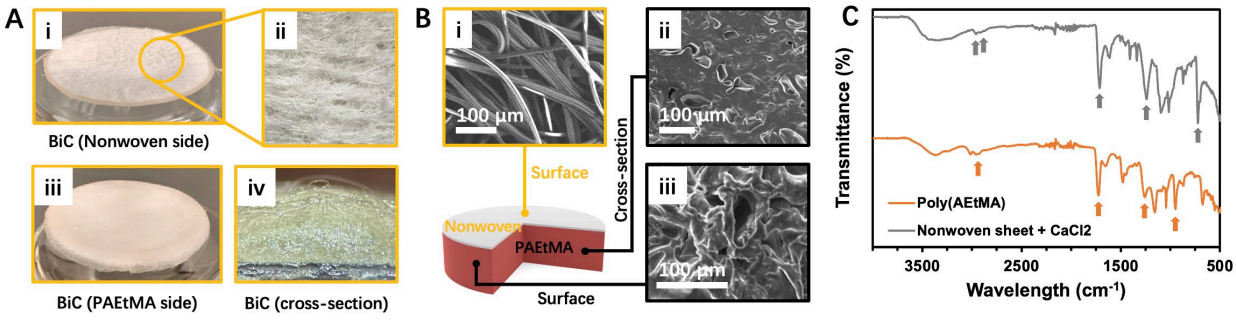


**Figure 1.** (A) Optic images of (i) surface of BiC (non-woven sheet side), (ii) optic microscopy image of non-woven fiber, (iii) the surface of BiC (polyAEtMA hydrogel side), (iv) optic microscopy image of the cross-section of BiC. (B) SEM images of (i) surface of non-woven sheet, (ii) cross-section and (iii) the surface of poly(AEtMA) hydrogel. (C) FT-IR spectra of the nonwoven sheet containing $CaCl_2$ (gray trace) and the PAEtMA hydrogel (orange trace).

The FT-IR spectra of the nonwoven substrate containing $CaCl_2$ and the obtained polymeric hydrogel layer were shown in Figure 1C. We observed the characteristic peaks at 1,250 $cm^{-1}$ and 1,750 $cm^{-1}$, which can be attributed to the carbonyl-stretching (C-O and C=O, respectively) of the PET nonwoven sheet. With the introduction of $CaCl_2$ in the nonwoven sheet, we observed a distinct broad water peak at 3,000 to 3,700 $cm^{-1}$. This suggests that the $CaCl_2$ in the nonwoven sheet adsorbed water during the test. From the FT-IR spectrum of the PAEtMA hydrogel (orange trace), we observed the characteristic peaks at 1,480 $cm^{-1}$ and 2,950 $cm^{-1}$, which are attributed to the stretching vibrations of $N^{+}$-C and C-H bonds of quaternary

ammonium groups of PAEtMA, respectively. These results confirmed the successful preparation of BiC containing $CaCl_2$.

We then evaluated the effects of the hygroscopic salts and the polymer hydrogels on the water production ability of BiCs though the vapor adsorption and desorption tests using a home-made setup. In the water adsorption experiments, BiC was placed in a plastic container immersed in an ice bath without touching the inner wall of the container (Figure 2A). The humidity (30-60% R.H.) is controlled by passing the dry air through different saturated salt solutions. Moist air with a fixed flow rate of 3.0 L $min^{-1}$ and a fixed relative humidity flows in from the top of the container. During sunlight-assisted water desorption, BiCs were placed on a precision balance under the irradiation of a simulate sunlight (intensity = 1 kW $m^{-2}$, Figure 2B). Under optimal conditions, BiC can raise its PAEtMA hydrogel surface temperature up to 40.4 °C within 4 hours for photothermal evaporation (see Supporting Information Figure S2).

We first optimized the loading of hygroscopic salts in BiC by tuning the concentration of the salt solution. In this study, we also prepared a control PAEtMA hydrogel without the nonwoven layer. As shown in Figure 2C, the bare PAEtMA hydrogel (HG-1, red trace) showed a water adsorption capacity of ca. 0.85 g $g^{-1}$ under 60% R.H. While, when we introduced $CaCl_2$ into PAEtMA hydrogel, the resulting hybrid AWH material (HG-2, green trace) showed a water adsorption capacity of ca. 0.9 g $g^{-1}$. Interestingly, the HG-2 exhibited rapid water adsorption rate in the first 2 hours, after which its adsorption rate gradually decreased. The amount of

water collected in the first two hours accounts for ca. 67% of the total water adsorption in the 12-hours water adsorption process. The rapid water adsorption is the result of the direct contact of water vapor and the hygroscopic salts and the quaternary ammonium groups. The subsequent decrease in water adsorption rate can be attributed to the formation of a saturated salt solution on the surface of the hygroscopic salts, resulting in an increase in vapor pressure, thereby inhibiting rapid liquefaction of water molecules. In contrast, the BiC with nonwoven-$CaCl_2$ (orange trace, 1M $CaCl_2$ solution, denoted as BiC-1) displayed an improved water liquefaction capacity, resulting in a higher water adsorption capacity of ca. 1.24 g $g^{-1}$ within the same time frame. This is because the liquefied water would be transferred and stored in the PAEtMA hydrogel layer. This result thus proves that an independent water liquefaction layer containing hygroscopic salt can effectively enhance the water adsorption capacity of an AWH material. In addition, we found that further increasing the concentration of $CaCl_2$ solution (from 1 mol $L^{-1}$ to 2 mol $L^{-1}$, denoted as BiC-2, yellow trace) did not significantly improve the water adsorption capacity. For BiC-2, due to its high hygroscopic salt content and strong hydrogen bonding between the hygroscopic salt and liquefied water, the transfer of liquefied water from WAL to the underlying PAEtMA is slower, which hinders the subsequent liquefaction of water vapor. During the subsequent water release, we observed that the BiC-2 showed lower water release efficiency than that of BiC-1, which could be attributed to its higher salt loading and stronger interaction with water molecules.

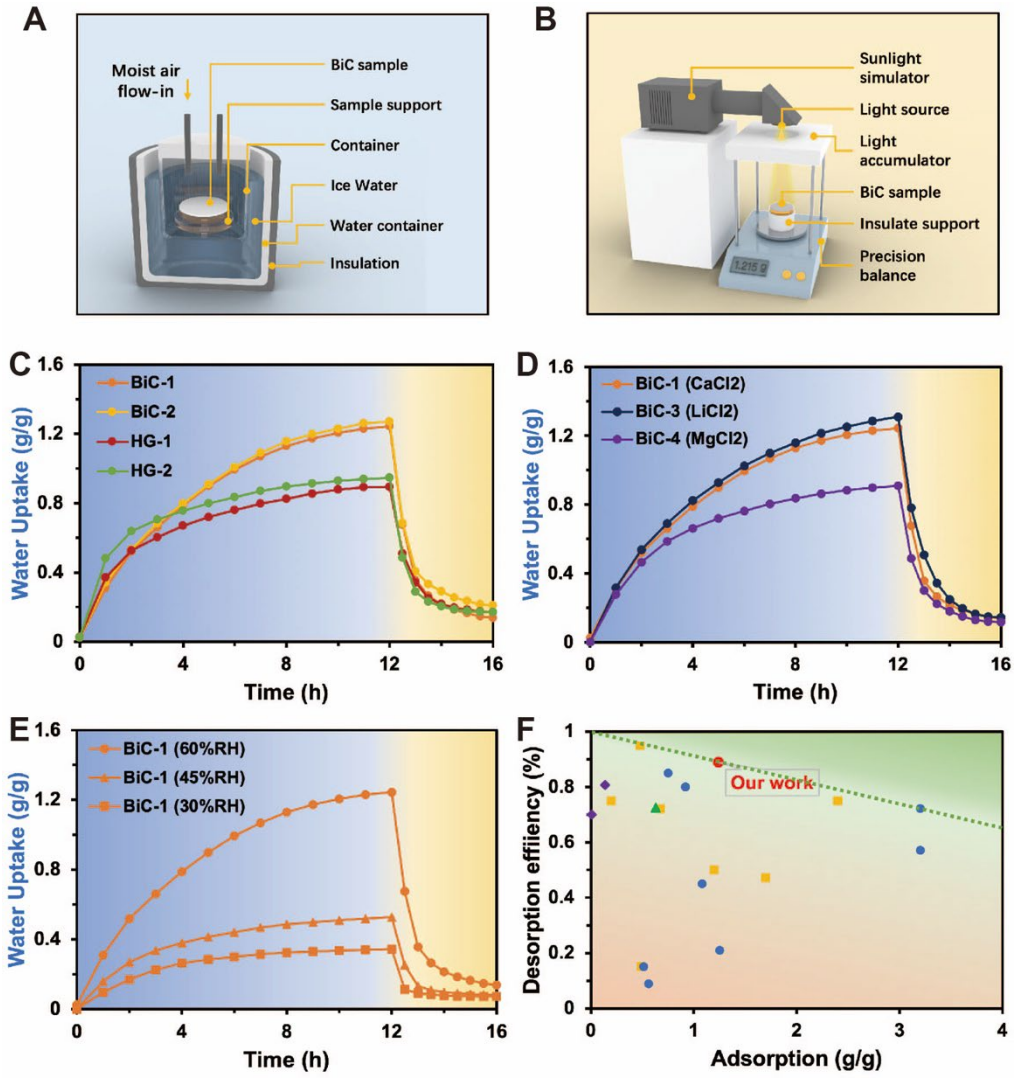


**Figure 2.** (A-B) Illustration of water adsorption and water desorption experiments, respectively. (C) In-door moisture capture and water release experiments of BiC-1 (orange trace), BiC-2 (yellow trace), HG-1 PAEtMA hydrogel (red trace) and HG-2 PAEtMA/$CaCl_2$ hybrid material (green trace). (D) Comparison of the in-door moisture capture and water release experiments of BiC-1 (1M $CaCl_2$ orange trace), BiC-3 (1M $LiCl_2$ dark blue trace), and BiC-4 (1M $MgCl_2$ purple trace) under 1.0 sun irradiation. (E) In-door moisture capture and water release experiments of BiC-1 at 30%, 45%, and 60% R.H. under 1.0 sun irradiation. (F) A trade-off (green dot line) between water adsorption capacity and water release efficiency of AWH materials: MOF and MOF composites (yellow rectangular)[17-24], HICs (purple

diamond)[25-27], ILs (green triangular)[28], and hydrogels (blue dots)[15, 16, 29-35].

We further optimize the water liquefaction ability of BiC by varying the types of hygroscopic salts. Apart from $CaCl_2$, we also introduced widely used LiCl and $MgCl_2$ into the nonwoven sheet to afford BiC samples (denoted as BiC-3 and BiC-4, respectively in Figure 2D). Compared with BiC-1, the BiC-3 containing LiCl exhibited 5.3% enhanced water adsorption capacity at the expense of 3.4% lower water release efficiency. Since we did not incorporate PTM into the BiC material, we focused more on the water release efficiency within a similar range of water adsorption capacity. On the other hand, the water adsorption capacity of BiC-1 is 136.9% of that of BiC-4 containing $MgCl_2$. Furthermore, we also directly compared the water liquefaction capacity of nonwoven sheets (not BiC) containing $CaCl_2$ and $MgCl_2$ and found that the nonwoven incorporating $CaCl_2$ exhibited higher water liquefaction capacity (ca. 115.2% improvement, see Supporting information S3). These results all indicate that the water adsorption capacity of BiCs is affected by hygroscopic salts.

Thereafter, we tested the water adsorption capacity of the BiC-1 under different R.H. conditions (30, 45 to 60% R.H.) at a moisture flow rate of 3 L $min^{-1}$. It is found that the water adsorption capacity of BiC-1 is 0.34, 0.53 and 1.24 g $g^{-1}$ at 30%, 45% and 60% R.H., respectively (Figure 2E). Compared with the low 30% R.H., the water adsorption capacity of BiC-1 increased by 261.8% at 60% R.H. This result demonstrates the potential of BiC for efficient water adsorption under arid environment compared with most hydrogel based AWH

materials, which typically displayed poor water adsorption capacity below 60% R.H.[10, 32, 34]

We also prepared another BiC consisting of the same nonwoven layer but poly(3-acrylamidopropyl)trimethylammonium chloride (PAPtMA) hydrogel layer and denoted it as BiC-5. Notably, both the PAEtMA- and PAPtMA-based hydrogel layers are rich in ammonium groups (see Supporting Information Figure S4A). The BiC-5 with PAPtMA hydrogel layer displayed a 14% lower water adsorption capacity. This result may be attributed to the higher molecular weight of the APtMA. Under the same polymer content, the PAEtMA network has more quaternary ammonium ions than that PAPtMA hydrogel layer. We then optimized the volume and density of the water-storage PAEtMA network and investigated this effect on the water adsorption capacity of BiC material. As mentioned above, we did not apply PTM in the preparation of BiCs, thus the excellent solar-assistant evaporation performance of BiC is attributed to its thin PAEtMA layer and high aspect ratio. We found that when we doubled the thickness of the PAEtMA polymer layer, water adsorption capacity of BiC-1 decreased from 1.24 g $g^{-1}$ to 0.56 g $g^{-1}$ (Supporting Information Figure S4B). Due to the constant water liquefaction rate of the WAL layer, filling a thicker PAGEMA layer with water requires a longer time (over 12 hours). However, the water adsorption process over 12 hours is not practical for AWH applications. Therefore, in this study, further increasing the thickness of the PAEtMA layer only increases the mass of BiC, significantly reducing the water adsorption capacity of BiC. Due to the difference in swelling ratio between nonwoven fiber and PAEtMA hydrogel, we must optimize the density of PAEtMA layer to control its mechanical stability and swelling ratio to find a balance between maintaining the structural integrity of BiCs and

maximizing their water absorption capacity. As shown in Figure S4C, when we further decreased the density of the PAEtMA layer to below 20 wt%, we observed an increase in water adsorption capacity, but the resulting PAEtMA network became brittle. On the other hand, further increasing the mass content of PAEtMA to 40 wt% led to a decrease in the swelling ratio and hence the water adsorption capacity per gram of BiC also decreased.

We further compared the AWH performance of BiC-1 with recently reported AWH materials (including metal-organic frameworks (MOFs) and their derivatives, hygroscopic inorganic compounds (HICs), ionic liquids (ILs), and hydrogels (Figure 2F). It is worth noting that in order to achieve high AWH performance, many studies reported using an air flow with higher R.H. as well as using a heating plate to drive evaporation. To be fair, we only compared the AWH data obtained under similar experimental conditions, e.g. below 60% R.H. and solar assisted evaporation. As seen, the MOF-based materials (yellow rectangular) generally exhibit high water adsorption capacity in low relative humidity environments, but have high residual water content even under sunlight irradiation. On the other hand, the hydrogel AWH materials (blue dots) generally show high sunlight-assisted desorption efficiency yet with a relatively low water adsorption capacity. As discussed above, the HICs (purple diamond) can quickly liquefy water vapor, but at the same time metal ions will dissolve in water to quickly form a saturated solution, preventing further moist liquefaction. In short, we can clearly observe a trade-off between the water adsorption capacity and the water release efficiency of AWH materials. In this study, the prepared BiC-1 exhibited excellent and balanced AWH performance, well ‘sitting’ at the frontline (aka. the upper bound) of the AWH trade-off.

Thereafter, we conducted durability tests to determine the structural stability and the AWH performance of the BiC-1 subjected to multiple water adsorption/desorption cycles using a home-made water harvesting device. The water is produced by sunlight-assisted evaporation and subsequent condensation process. Under sunlight irradiation the water condensed, formed droplets, then flow towards the bottom of container for collection (Figure 3A). After ten water adsorption and release cycles (total 120 hours), the obtained BiC-1 can still maintain its AWH performance with ca. 1.1 g $g^{-1}$ water adsorption capacity and 84.6% water release efficiency (Figure 3B). The evaporated water was subsequently condensed in the device, achieving a total 0.75 kg $kg^{-1}$ daily water production. The collected water was then characterized by ICP-MS to determine the salt concentration. The ion concentrations of Sydney tap water and laboratory deionized water were also measured for reference. As shown in Figure 3C, Sydney tap water had the highest $Na^{+}$ and $Ca^{2+}$ ion concentrations of 12.69 mg $L^{-1}$ and 11.69 mg $L^{-1}$ respectively, followed by laboratory deionized water (<0.01 mg $L^{-1}$ and 0.13 mg $L^{-1}$, respectively). The concentration of ions ($Na^{+}$, $Ca^{2+}$, $Mg^{2+}$ and $K^{+}$) in the collected water is the lowest among them. The calibration curves of all ions are shown in Figure S5 (Supporting Information).

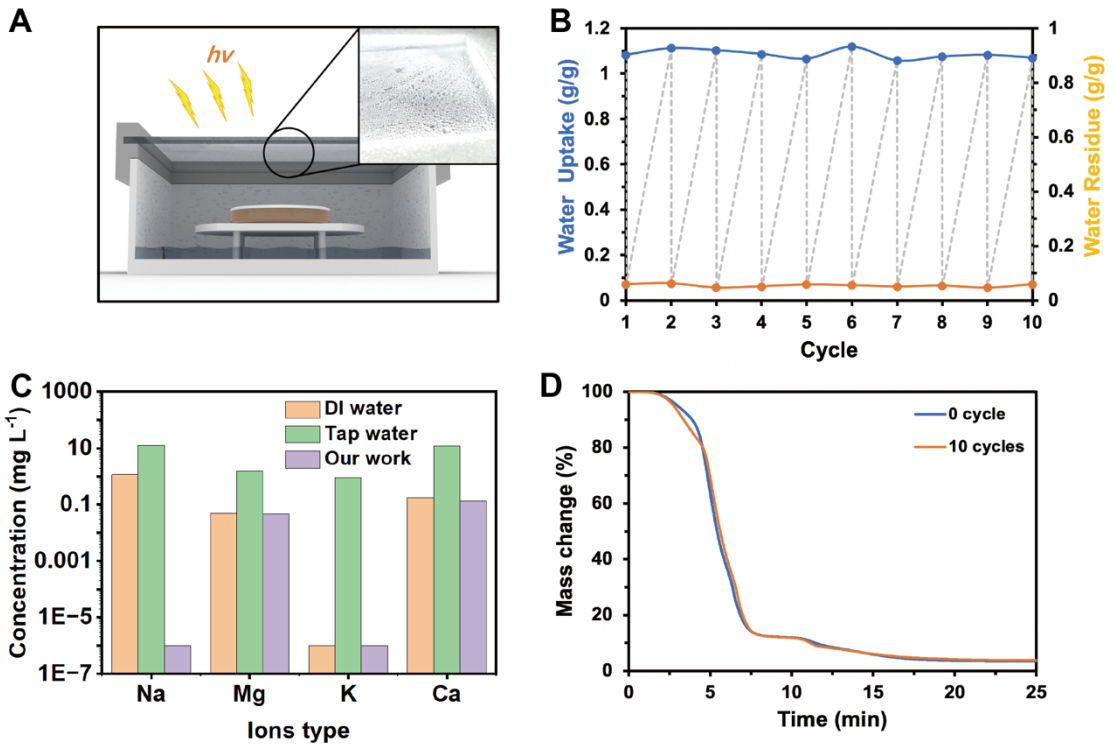


**Figure 3.** (A) Illustration of the home-made water harvesting device. (B) AWH performance of BiC-1 in 10-times cycling tests. (C) Ion concentrations of Sydney tap water, DI water and the collected water using BiC-1. (D) TGA curves for residue calcium chloride content in PAEtMA network before and after ten water adsorption/desorption cycles.

Due to different swelling ratios of the nonwoven sheet and the PAEtMA hydrogel layer, strong repulsive tension may be generated at their interface during the water adsorption-desorption processes. We thus characterized the cross-section morphology of the BiC-1 after cycling tests to determine its structural stability. As shown in Supporting Information Figure S6, the PAEtMA hydrogel layer is still closely attached to the nonwoven sheet without obvious gaps or detachment. Moreover, for hydrogel AWH materials, the incorporated hygroscopic salts have been reported to leach from the polymer matrix to the produced water, resulting in performance decay and potentially environmental contamination issues[14]. For the BiC system,

because the liquefied water finally flows to the PAEtMA hydrogel layer, we performed TGA measurements to verify if any $CaCl_2$ leached to the hydrogel layer. The as-prepared PAEtMA hydrogel layer of BiC-1 was measured by TGA first (blue trace, Figure 3D). After ten water adsorption-release cycles, the hydrogel layer of the BiC-1 was also removed, dried and characterized by TGA (orange trace). Interestingly, the two TGA traces are almost identical, the orange one shows only a slight increase (< 0.06 wt%) in the weight ratio of the residue. This result indicates that during the AWH processes, most of the $CaCl_2$ was retained in the nonwoven sheet of BiC material thus ensuring its high durability and stable AWH performance.

## CONCLUSION

Inspired by the water capture process of Tillandsia air-plants, we developed an artificial composite material for efficient water production in low-moderate humidity (<60% RH) environments. The nonwoven surface treated with hygroscopic salts is applied to liquefy water vapor, and the PAEtMA hydrogel network beneath the nonwoven sheet has high porosity and a high swelling ratio for liquid water storage. The porous structure generates capillary force to drive the transport of liquid water from the nonwoven surface into the PAEtMA network. In addition, we also found that the BiC system can prevent the potential leaching of hygroscopic salts. We thus believe that the reported BiC material offers an alternative pathway for efficient AWH processes in harsh environments that do not require secondary energy and provides a potential solution for the recycling of discarded disposable masks in the post-COVID-19 era.

ASSOCIATED CONTENT

SI Supporting Information

The supporting information is available as an individual document provided with this article. Experimental section, Optic and SEM images, Thermal camera images, Water adsorption process of hygroscopic salts, supplementary AWH performance, calibration curves.

AUTHOR INFORMATION

**Corresponding Author**

*E-mail: qiang.fu@uts.edu.au (Q. Fu).

**ORCID**

An Feng: 0000-0002-8444-798X

Shudi Mao: 0000-0002-4761-4670

Casey Onggowarsito: 0000-0002-8962-7971

Gayathri Danasamy: 0000-0002-6406-3444

Wen Li: 0000-0002-3851-7406

Qiang Fu: 0000-0002-4012-330X

**Notes**

The authors declare no competing financial interest.

ACKNOWLEDGMENT

Q. F. acknowledges the Australian Research Council under the Future Fellowship (FT180100312). A. F. acknowledges support of the International Research Scholarship from the University of Technology Sydney.

REFERENCES

1. Moszynski, P., Worldwide water crisis is a “silent emergency,” UN agency says. *BMJ* **2006,** *333* (7576), 986-986. DOI: 10.1136/bmj.333.7576.986-a.

2. Singh, R., Worldwide water crisis. *Journal of membrane science* **2008,** *313* (1), 353-354. DOI: 10.1016/j.memsci.2008.01.016.

3. Barbier, E., *The Water Paradox: Overcoming the Global Crisis in Water Management*. Yale University Press: New Haven, 2019.

4. Li, Q.; Ying, Y.; Tao, Y.; Li, H., Assemblable Carbon Fiber/Metal–Organic Framework Monoliths for Energy-Efficient Atmospheric Water Harvesting. *Industrial & engineering chemistry research* **2022,** *61* (3), 1344-1354. DOI: 10.1007/s00339-021-04619-1.

5. Sun, H.; Song, Y.; Zhang, B.; Huan, Y.; Jiang, C.; Liu, H.; Bao, T.; Yu, S.; Wang, H., Bioinspired micro- and nanostructures used for fog harvesting. *Applied physics. A, Materials science & processing* **2021,** *127* (6). DOI: 10.1007/s00339-021-04619-1.

6. Hu, Y.; Fang, Z.; Wan, X.; Ma, X.; Wang, S.; Fan, S.; Dong, M.; Ye, Z.; Peng, X., Carbon nanotubes decorated hollow metal–organic frameworks for efficient solar-driven atmospheric water harvesting. *Chemical engineering journal (Lausanne, Switzerland : 1996)* **2022,** *430*, 133086. DOI: 10.1016/j.cej.2021.133086.

7. Silva, M. P.; Ribeiro, A. M.; Silva, C. G.; Ho Cho, K.; Lee, U. H.; Faria, J. L.; Loureiro, J. M.; Chang, J.-S.; Rodrigues, A. E.; Ferreira, A., Atmospheric water harvesting on MIL-100(Fe) upon a cyclic adsorption process. *Separation and purification technology* **2022,** *290*, 120803. DOI: 10.1016/j.seppur.2022.120803.

8. Ha, N.; Park, J.; Park, S. H.; Seo, E.; Lim, J. H.; Lee, S. J., Domino-like water transport on Tillandsia through flexible trichome wings. *The New phytologist* **2021,** *231* (5), 1906-1922. DOI: 10.1111/nph.17336.

9. Miranda, T.; Roth-Nebelsick, A.; Junginger, A.; Ebner, M., Habitat conditions, spatial distribution and trichome morphology of different species of Tillandsia growing on trees on the Ilha Grande Island, Brazil. *Flora. Morphologie, Geobotanik, Oekophysiologie* **2020,** *272*, 151692. DOI: 10.1016/j.flora.2020.151692.

10. Allison-Logan, S.; Fu, Q.; Sun, Y.; Liu, M.; Xie, J.; Tang, J.; Qiao, G. G., From UV to NIR: A Full-Spectrum Metal-Free Photocatalyst for Efficient Polymer Synthesis in Aqueous Conditions. *Angewandte Chemie International Edition* **2020,** *59* (48), 21392-21396. DOI: https://doi.org/10.1002/anie.202007196.
11. Lu, H.; Shi, W.; Guo, Y.; Guan, W.; Lei, C.; Yu, G., Materials Engineering for Atmospheric Water Harvesting: Progress and Perspectives. *Advanced materials (Weinheim)* **2022,** *34* (12), e2110079-n/a. DOI: 10.1002/adma.202110079.
12. Hanikel, N.; Prévot, M. S.; Yaghi, O. M., MOF water harvesters. *Nature nanotechnology* **2020,** *15* (5), 348-355. DOI: 10.1038/s41565-020-0673-x.
13. Zhang, S.; Fu, J.; Das, S.; Ye, K.; Zhu, W.; Ben, T., Crystalline Porous Organic Salt for Ultrarapid Adsorption/Desorption - Based Atmospheric Water Harvesting by Dual Hydrogen Bond System. *Angewandte Chemie International Edition* **2022,** *61*(40), e202208660. DOI: 10.1002/ange.202208660.
14. Shan, H.; Pan, Q.; Xiang, C.; Poredoš, P.; Ma, Q.; Ye, Z.; Hou, G.; Wang, R., High-yield solar-driven atmospheric water harvesting with ultra-high salt content composites encapsulated in porous membrane. *Cell reports physical science* **2021,** *2* (12), 100664. DOI: 10.1016/j.xcrp.2021.100664.
15. Li, R.; Shi, Y.; Alsaedi, M.; Wu, M.; Shi, L.; Wang, P., Hybrid Hydrogel with High Water Vapor Harvesting Capacity for Deployable Solar-Driven Atmospheric Water Generator. *Environmental science & technology* **2018,** *52* (19), 11367-11377. DOI: 10.1021/acs.est.8b02852.
16. Zhao, F.; Zhou, X.; Liu, Y.; Shi, Y.; Dai, Y.; Yu, G., Super moisture-absorbent gels for all-weather atmospheric water harvesting. *Advanced Materials* **2019,** *31* (10), 1806446. DOI: 10.1002/adma.201806446.
17. Rieth, A. J.; Wright, A. M.; Skorupskii, G.; Mancuso, J. L.; Hendon, C. H.; Dincă, M., Record-Setting Sorbents for Reversible Water Uptake by Systematic Anion Exchanges in Metal−Organic Fra meworks. *Journal of the American Chemical Society* **2019,** *141* (35), 13858-13866. DOI: 10.1021/jacs.9b06246.
18. Towsif Abtab, S. M.; Alezi, D.; Bhatt, P. M.; Shkurenko, A.; Belmabkhout, Y.; Aggarwal, H.; Weseliński, Ł. J.; Alsadun, N.; Samin, U.; Hedhili, M. N.; Eddaoudi, M., Reticular Chemistry in Action: A Hydrolytically Stable MOF Capturing Twice Its Weight in Adsorbed Water. *Chem* **2018,** *4* (1), 94-105. DOI: 10.1016/j.chempr.2017.11.005.
19. Kim, H.; Yang, S.; Rao, S. R.; Narayanan, S.; Kapustin, E. A.; Furukawa, H.; Umans, A. S.; Yaghi, O. M.; Wang, E. N., Water harvesting from air with metal-organic frameworks powered by natural sunlight. *Science (American Association for the Advancement of Science)* **2017,** *356* (6336), 430-434. DOI: 10.1126/science.aam8743.
20. Hu, Y.; Fang, Z.; Ma, X.; Wan, X.; Wang, S.; Fan, S.; Ye, Z.; Peng, X., CaCl2 Nanocrystals decorated photothermal Fe-ferrocene MOFs hollow microspheres for atmospheric water harvesting. *Applied materials today* **2021,** *23*, 101076. DOI: 10.1016/j.apmt.2021.101076.
21. Li, R.; Shi, Y.; Wu, M.; Hong, S.; Wang, P., Improving atmospheric water production yield: Enabling multiple water harvesting cycles with nano sorbent. *Nano energy* **2020,** *67*, 104255. DOI: 10.1016/j.nanoen.2019.104255.
22. Maher, H.; Rupam, T. H.; Rocky, K. A.; Bassiouny, R.; Saha, B. B., Silica gel-MIL 100(Fe) composite adsorbents for ultra-low heat-driven atmospheric water harvester. *Energy (Oxford)* **2022,** *238*, 121741. DOI: 10.1016/j.energy.2021.121741.
23. Wu, Q.; Su, W.; Li, Q.; Tao, Y.; Li, H., Enabling Continuous and Improved Solar-Driven Atmospheric Water Harvesting with Ti3C2 - Incorporated Metal−Organic Framework Monoliths. *ACS applied materials & interfaces* **2021,** *13* (32), 38906-38915. DOI: 10.1021/acsami.1c10536.
24. Tao, Y.; Li, Q.; Wu, Q.; Li, H., Embedding metal foam into metal-organic framework monoliths for

triggering a highly efficient release of adsorbed atmospheric water by localized eddy current heating. *Materials horizons* **2021,** *8* (5), 1439-1445. DOI: 10.1039/d1mh00306b.

25. Wang, J.; Dang, Y.; Meguerdichian, A. G.; Dissanayake, S.; Kankanam-Kapuge, T.; Bamonte, S.; Tobin, Z. M.; Achola, L. A.; Suib, S. L., Water Harvesting from the Atmosphere in Arid Areas with Manganese Dioxide. *Environmental science & technology letters* **2020,** *7* (1), 48-53. DOI: 10.1021/acs.estlett.9b00713.

26. Wang, X.; Li, X.; Liu, G.; Li, J.; Hu, X.; Xu, N.; Zhao, W.; Zhu, B.; Zhu, J., An Interfacial Solar Heating Assisted Liquid Sorbent Atmospheric Water Generator. *Angewandte Chemie International Edition* **2019,** *58*(35), 12054-12058. DOI: 10.1002/ange.201905229.

27. Liu, X. Y.; Wang, W. W.; Xie, S. T.; Pan, Q. W., Performance characterization and application of composite adsorbent LiCl@ACFF for moisture harvesting. *Scientific reports* **2021,** *11* (1), 14412-14412. DOI: 10.1038/s41598-021-93784-7.

28. Qi, H.; Wei, T.; Zhao, W.; Zhu, B.; Liu, G.; Wang, P.; Lin, Z.; Wang, X.; Li, X.; Zhang, X.; Zhu, J., An Interfacial Solar-Driven Atmospheric Water Generator Based on a Liquid Sorbent with Simultaneous Adsorption–Desorption. *Advanced materials (Weinheim)* **2019,** *31* (43), e1903378. DOI: 10.1002/adma.201903378.

29. Yilmaz, G.; Meng, F. L.; Lu, W.; Abed, J.; Peh, C. K. N.; Gao, M.; Sargent, E. H.; Ho, G. W., Autonomous atmospheric water seeping MOF matrix. *Science advances* **2020,** *6* (42), eabc8605. DOI: 10.1126/sciadv.abc8605.

30. Entezari, A.; Ejeian, M.; Wang, R., Super Atmospheric Water Harvesting Hydrogel with Alginate Chains Modified with Binary Salts. *ACS materials letters* **2020,** *2* (5), 471-477. DOI: 10.1021/acsmaterialslett.9b00315.

31. Kabir, A.; Dunlop, M. J.; Acharya, B.; Bissessur, R.; Ahmed, M., Water recycling efficacies of extremely hygroscopic, antifouling hydrogels. *RSC advances* **2018,** *8* (66), 38100-38107. DOI: 10.1039/c8ra07915c.

32. Wu, M.; Li, R.; Shi, Y.; Altunkaya, M.; Aleid, S.; Zhang, C.; Wang, W.; Wang, P., Metal- and halide-free, solid-state polymeric water vapor sorbents for efficient water-sorption-driven cooling and atmospheric water harvesting. *Materials horizons* **2021,** *8* (5), 1518-1527. DOI: 10.1039/d0mh02051f.

33. Lei, C.; Guo, Y.; Guan, W.; Lu, H.; Shi, W.; Yu, G., Polyzwitterionic Hydrogels for Efficient Atmospheric Water Harvesting. *Angewandte Chemie International Edition* **2022,** *61*(13), e202200271. DOI: 10.1002/ange.202200271.

34. Karmakar, A.; Mileo, P. G. M.; Bok, I.; Peh, S. B.; Zhang, J.; Yuan, H.; Maurin, G.; Zhao, D., Thermo-Responsive MOF/Polymer Composites for Temperature-Mediated Water Capture and Release. *Angewandte Chemie International Edition* **2020,** *59*, 11003. DOI: 10.1002/ange.202002384.

35. Chen, B.; Zhao, X.; Yang, Y., Superelastic Graphene Nanocomposite for High Cycle-Stability Water Capture–Release under Sunlight. *ACS applied materials & interfaces* **2019,** *11* (17), 15616-15622. DOI: 10.1021/acsami.9b02215.

TABLE OF CONTENTS (TOC) GRAPHIC

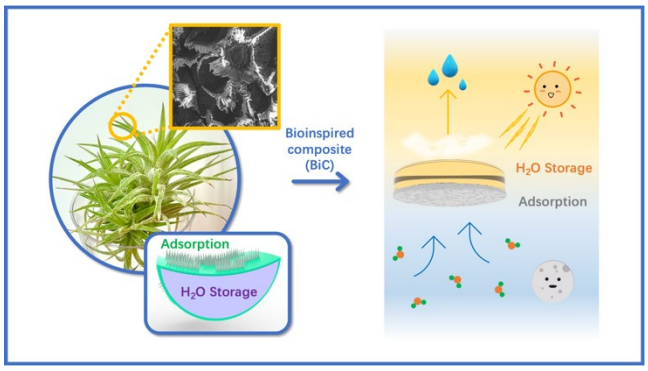


This Tillandsia-inspired BiC material is suitable for all weather AWH, and helps reduce the negative impact of global water crisis.

(For Table of Contents Use Only.)